Methylammonium Lead Bromide Perovskite-Based Solar Cells by Vapor-Assisted Deposition

ARTICLE *in* THE JOURNAL OF PHYSICAL CHEMISTRY C · FEBRUARY 2015

Impact Factor: 4.77 · DOI: 10.1021/jp512936z

7 AUTHORS, INCLUDING:

Rui Sheng
University of New South Wales
12 PUBLICATIONS **39** CITATIONS
SEE PROFILE

Xiaoming Wen
University of New South Wales
103 PUBLICATIONS **694** CITATIONS
SEE PROFILE

Xiaojing Hao
University of New South Wales
76 PUBLICATIONS **886** CITATIONS
SEE PROFILE

Martin Green
University of New South Wales
720 PUBLICATIONS **24,602** CITATIONS
SEE PROFILE

THE JOURNAL OF PHYSICAL CHEMISTRY C

Article

pubs.acs.org/JPCC

Methylammonium Lead Bromide Perovskite-Based Solar Cells by Vapor-Assisted Deposition

Rui Sheng, Anita Ho-Baillie,* Shujuan Huang, Sheng Chen, Xiaoming Wen, Xiaojing Hao, and Martin A. Green

Australian Centre for Advanced Photovoltaics (ACAP) School of Photovoltaic and Renewable Energy Engineering, University of New South Wales, Sydney 2052, Australia

Supporting Information

ABSTRACT: The past two years have seen the uniquely rapid emergence of a new class of solar cell based on organic−inorganic halide perovskite. Although less explored than its tri-iodide counterparts, $CH_3NH_3PbBr_3$ has a larger bandgap of 2.3 eV with a higher voltage potential that is suitable for tandem solar cell applications. In this paper, we report a vapor-assisted method for depositing and fully crystallizing $CH_3NH_3PbBr_3$ film on mesoporous TiO_2 with good coverage. $CH_3NH_3PbBr_3$ fabricated using this method has demonstrated long carrier diffusion length (>1 μm) as estimated by transient photoluminescence-quenching measurements. We demonstrate solar cells fabricated using such films and spiro-OMeTAD as the hole transport layer with an averaged (from forward and reverse scans) conversion efficiency of 8.7%, V_{oc} of 1.45 V, J_{sc} of 9.75 mA/cm^2, and fill factor of 61.5%.

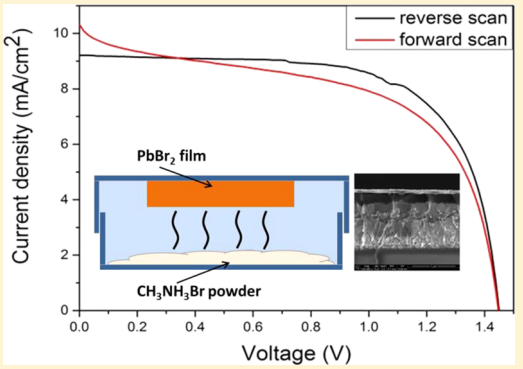

Methylammonium lead halide perovskite solar cells have attracted enormous research interests in the past two years.[1,2] Much of the attention is focused on $CH_3NH_3PbI_3$ or mixed halides $CH_3NH_3PbI_{3-x}Cl_x$ and $CH_3NH_3PbI_{3-x}Br_x$ devices with a bandgap in the vicinity of 1.6 eV, despite the first reported photovoltaic results for perovskites were based on $CH_3NH_3PbBr_3$.[3] The advantage of higher bandgap (2.3 eV) and therefore larger voltage potential of bromide-based perovskite makes it a promising candidate for a tandem system,[4] such as a three-cell stack. The highest efficiency of 10.4% has been reported by using the crystallization-controlled spin-coating process and poly(indenofluoren-8-triarylamine) (PIF8-TAA) as hole transport layer.[5] Other works demonstrating efficient $CH_3NH_3PbBr_3$ perovskite solar device employ poly(3-hexyl)thiophene (P3HT), *N,N′*-bis(3-methylphenyl)-*N,N′*-diphenylbenzidine (TPD), [6,6]-phenyl-C61-butyric acid methyl ester (PCBM), *N,N′*-dialkylperylenediimide (PDI), or poly(triarylamine) (PTAA) as hole transport materials.[6−8] The $CH_3NH_3PbBr_3$ films in these works are deposited using the solution-based method. Here we demonstrate a solar device based on $CH_3NH_3PbBr_3$ perovskite deposited via a vapor-assisted crystallization method employing spiro-OMeTAD as a hole transport material.

Various deposition techniques have been used for the fabrication of methylammonium lead halide perovskite solar cells. One of the challenges associated with the one-step precursor solution spin-coating process is the lack of suitable solvents that can dissolve the components in the precursor mixture and the high reaction rate of the perovskite components resulting in incomplete coverage and poor uniformity,[9−12] leading to low-resistance shunting paths and loss of light absorption in the solar cells.[10] Chloride inclusion, optimization of annealing conditions, and the sequential solution-based deposition method have been demonstrated to increase film coverage and uniformity.[10,13,14] Dual-source vacuum evaporation has also been employed allowing efficient perovskite solar device to be fabricated with excellent film coverage and uniformity,[15] but the high-vacuum requirement precludes this method from mass adoption. Although the vapor-assisted method has been used to fabricate planar $CH_3NH_3PbI_3$ perovskite solar cells,[9] it has not been employed in a cell structure where a mesoporous layer is present. The planar perovskite cell structure without the mesoporous layer has the advantage of a simplified design reducing number of fabrication steps and simplifying the design.[5] This may potentially be beneficial for tandem cell construction and allows the investigation of the underlying device physics[9] without the complication of the mesoporous layer. However, recent research has reported that the presence of mesoporous layer, in particular the mesoporous TiO_2 (mp-TiO_2) when its thickness is optimized, is beneficial in reducing the hysteresis in perovskite solar cells compared with planar structure.[16,17]

In this work, we report the fabrication of high-voltage $CH_3NH_3PbBr_3$ solar cell using the vapor-assisted deposition method on a mp-TiO_2 scaffold employing spiro-OMeTAD as a hole transport material. The perovskite film exhibits densely

Received: December 28, 2014
Revised: January 25, 2015

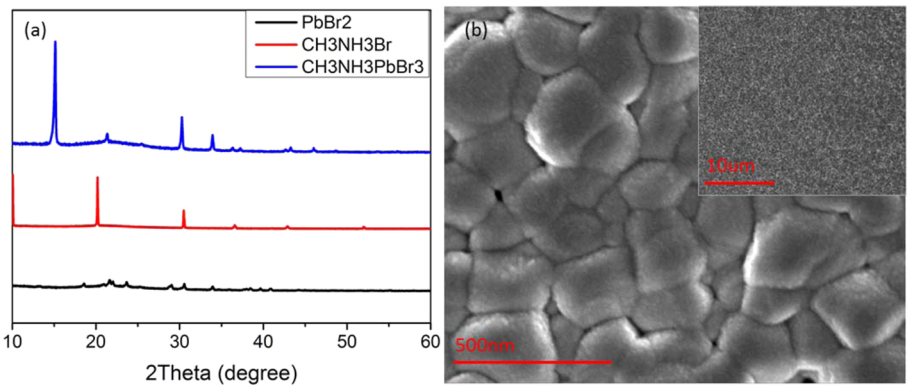

Figure 1. (a) XRD pattern of $CH_3NH_3PbBr_3$ film deposited by the vapor-assisted method compared with that of CH_3NH_3Br and $PbBr_2$ films as references. (b) SEM top view of vapor-assisted deposited $CH_3NH_3PbBr_3$ film.

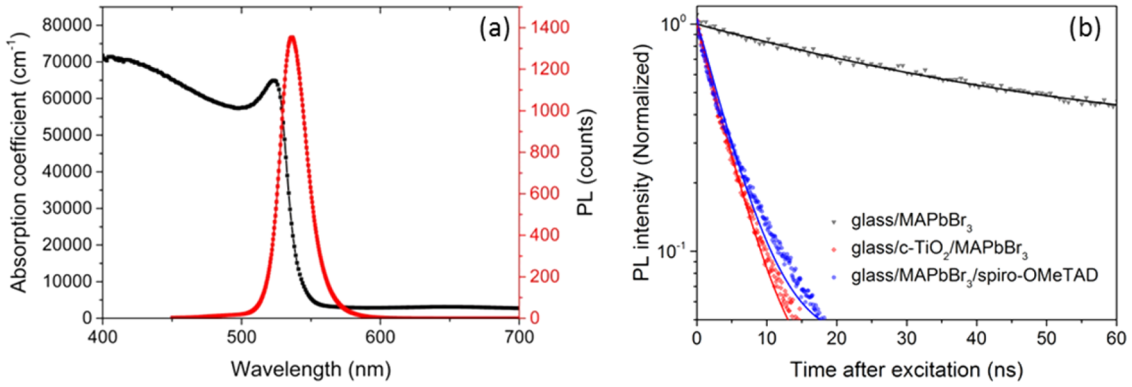

Figure 2. (a) Absorption coefficient (black) and PL spectrum (red) of the $CH_3NH_3PbBr_3$ film. (b) tr-PL taken at emission wavelength of 536 ± 10 nm for samples with and without quenchers: glass/$CH_3NH_3PbBr_3$ (black), glass/c-TiO_2/$CH_3NH_3PbBr_3$ (blue), and glass/$CH_3NH_3PbBr_3$/spiro-OMeTAD (red). The solid lines represent the stretched exponential fit for glass/$CH_3NH_3PbBr_3$ PL data and diffusion model fits for the $CH_3NH_3PbBr_3$ in the presence of quenchers.

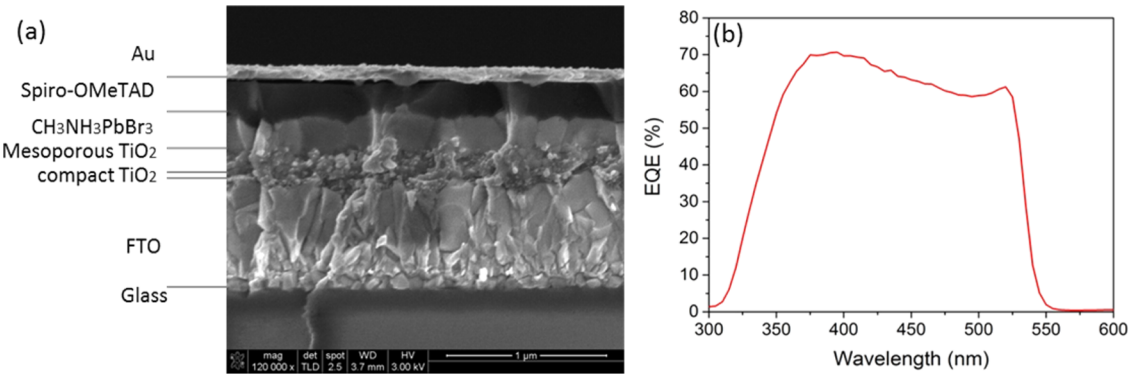

Figure 3. (a) SEM cross-sectional image (b) external quantum efficiency of a complete device.

packed grains and excellent coverage, in particular when it is a capping layer, over the mp-TiO_2 surface. Solar devices based on this structure have achieved power conversion efficiency of 8.7% (average value of forward and reverse scans). In addition, carrier dynamics of the $CH_3NH_3PbBr_3$ films was studied using photoluminescence-quenching measurements.

Figure 1a shows the X-ray diffraction (XRD) patterns of a $CH_3NH_3PbBr_3$ (blue) film deposited by the vapor-assisted method as well as CH_3NH_3Br (red) and $PbBr_2$ (black) films for reference. All of the films are deposited on mp-TiO_2/compact TiO_2 (c-TiO_2)/ glass. The XRD pattern of $CH_3NH_3PbBr_3$ indicates a cubic perovskite phase has formed,[6] where the peaks of (100) at 14.87°, (110) at 21.33°, (200) at 30.29°, (220) at 42.87°, and (300) at 48.21° are present. CH_3NH_3Br and $PbBr_2$ residuals are not detected in the synthesized $CH_3NH_3PbBr_3$, indicating after all of the $PbBr_2$ is converted into $CH_3NH_3PbBr_3$, the remaining CH_3NH_3Br has been removed completely during solvent evaporation. As shown in the top-view scanning electron microscopy (SEM) image in Figure 1b, $CH_3NH_3PbBr_3$ film deposited by the vapor-assisted method is uniform with densely packed grains (sizes range from 200 to 300 nm) with full coverage.

The absorption coefficient in Figure 2a and the photoluminescence (PL) of the film with a peak at 536 nm in Figure

DOI: 10.1021/jp512936z
J. Phys. Chem. C XXXX, XXX, XXX−XXX

Table 1. Experimentally Determined Diffusion Coefficient (D) and Diffusion Lengths (L_D) of $CH_3NH_3PbBr_3$ Film in This Work

absorption coeff at 470 nm (cm^{-1})	thickness (nm)	τ_e (ns)	charge species	D ($cm^2\ s^{-1}$)	L_D (nm)
6×10^4	480 ± 20	51	negative	0.2198 ± 0.02	1058 ± 48
			positive	0.2301 ± 0.02	1083 ± 47

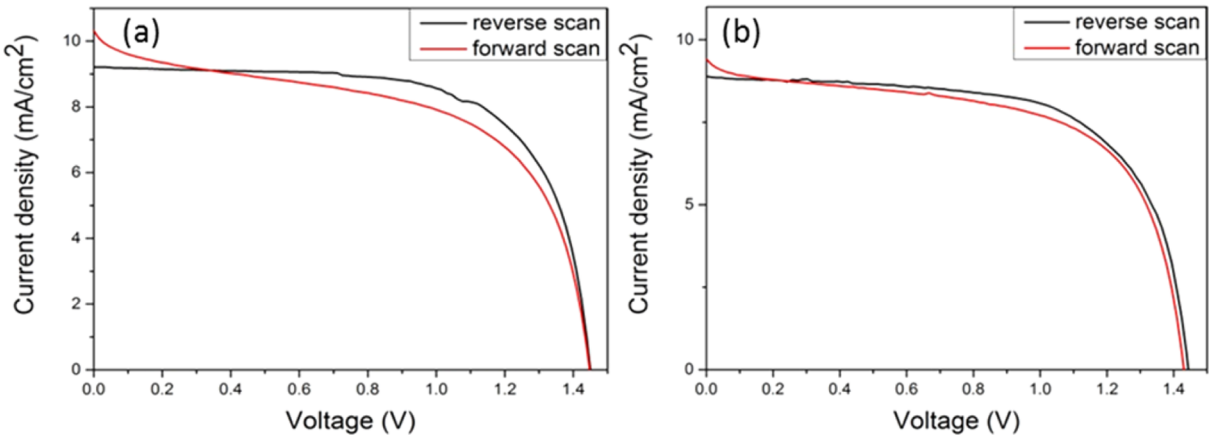

Figure 4. Current density−voltage curves measured in opposite sweeping directions at a rate of (a) 3 and (b) 0.15 V/s.

Table 2. Electrical Characteristics of the Same Device As Shown in Figure 4 Measured under Different Scan Speeds and Sweeping Directions

deposition method used	scan	V_{oc} (V)	J_{sc} (mA/cm^2)	FF (%)	R_S (ohm·cm^2)	R_{SH} (ohm·cm^2)	eff (%)
vapor-assisted	3 V/s reverse	1.45	9.2	68	190	5.7×10^4	9.1
vapor-assisted	3 V/s forward	1.45	10.3	55	3171	3.7×10^3	8.3
vapor-assisted	0.15 V/s reverse	1.44	8.9	64	188	6.5×10^3	8.4
vapor-assisted	0.15 V/s forward	1.43	9.4	60	4573	5.5×10^3	8.1

2b reveal a bandgap of 2.31 eV, which is consistent with that reported in other work.[18] Time-resolved photoluminescence (tr-PL) spectra taken at emission wavelength of 536 ± 10 nm for glass/$CH_3NH_3PbBr_3$ (black), glass/c-TiO_2/$CH_3NH_3PbBr_3$ (blue), and glass/$CH_3NH_3PbBr_3$/spiro-OMeTAD (red) together with the stretched exponential fit (in the absence of quencher) and diffusion model fits (in the presence of quenchers of TiO_2 and spiro-OMeTAD) are shown in Figure 2b. A near-band-edge peak observed in absorption (see Figure 2a) and in EQE curve of a complete device in Figure 3b suggests exciton absorption, which is feasible given a reported binding energy of 76 meV[20] for this material and similar diffusion coefficient and diffusion length for different charge species reported in this work. Using the models described by eq 4, the carrier lifetime of the $CH_3NH_3PbBr_3$ film is experimentally determined to be τ_e = 51 ns while the lifetimes of the $CH_3NH_3PbBr_3$ film in the presence of quencher of TiO_2 and spiro-OMeTAD are 3.5 and 3.1 ns, respectively. A commonly used diffusion model as described by eq 5 is used to extract the diffusion coefficient from the tr-PL data by calculating the distribution of photoexcited charge carriers using models described by eq 6.[21−23] The diffusion length of $CH_3NH_3PbBr_3$ estimated in this work is around 1 μm, higher than that reported.[24] This is due to better crystallinity in the $CH_3NH_3PbBr_3$ film with no CH_3NH_3Br and $PbBr_2$ residuals as no solvent is involved in the vapor deposition of CH_3NH_3Br. However, this is not the case for the $CH_3NH_3PbBr_3$ film reported in the literature,[24] whereby CH_3NH_3Br residuals can be detected due to the complication of solvent involved the solution deposition of CH_3NH_3Br. The higher lifetime reported in this work compared to other work[23] also contributes to better electrical characteristics of the complete device. The experimentally determined diffusion coefficients and diffusion length of the $CH_3NH_3PbBr_3$ film in this work are summarized in Table 1.

Figure 3a shows the cross-sectional SEM image of the complete device with the structure of FTO glass/c-TiO_2/mp-TiO_2/$CH_3NH_3PbBr_3$/spiro-OMeTAD/Au. To fabricate such structure, 40 nm of c-TiO_2 hole blocking layer was spin-coated on a commercially available fluorine-doped tin oxide (FTO, Pilkington, TEC8) glass substrate. A 350 nm thick mp-TiO_2 film was then deposited by spin-coating a diluted colloidal anatase paste to form the electron-extracting scaffold. The light absorber, $CH_3NH_3PbBr_3$, was then fabricated by the vapor-assisted method. After annealing, the spiro-OMeTAD was spin-coated as HTM before thermal deposition of gold contact.

As can be seen, a dense and uniform capping layer of $CH_3NH_3PbBr_3$ 325 ± 75 nm in thickness is formed above the mp-TiO_2 scaffold layer. This method appears to be superior compared with the solution-based method whereby pillared overlayer has been observed[6] and uniformity is difficult to be controlled (see Figure S2 when the $CH_3NH_3PbBr_3$ film is prepared by the solution-based method).

The electrical characteristics of a solar device are shown in Figure 4 and Table 2. Averaged (from forward and reverse scans) conversion efficiency of 8.7%, V_{oc} of 1.45 V, J_{sc} of 9.75 mA/cm^2, and fill factor of 61.5% results show that the device exhibits stronger hysteresis under fast scans. Compared with one-step solution processed $CH_3NH_3PbBr_3$ device (see Figure S4 and Table S1 in the Supporting Information), the vapor-assisted deposited $CH_3NH_3PbBr_3$ device exhibits a smaller degree of hysteresis. The current and spectral response (see

DOI: 10.1021/jp512936z
J. Phys. Chem. C XXXX, XXX, XXX−XXX

Figure 3b) demonstrated the effectiveness of the $CH_3NH_3PbBr_3$ prepared by the vapor-assisted method as a light absorber (with a bandgap of 2.31 eV, consistent with that deduced from experimental absorption coefficient in Figure 2a). A respectrable V_{oc} has been shown to be an indicator of film quality, in particular its surface coverage,[6] either in planar structure or as capping layer on a scaffold,[25] as supported by SEM evidence in this work. An open circuit voltage of 1.44 ± 0.01 V and averaged FF of ∼62% have been achieved for some devices. The fill factor from this study demonstrates that spiro-OMeTAD is effective in extracting holes from the $CH_3NH_3PbBr_3$ film. The high R_{SH} of $>10^3$ ohm·cm^2 measured also indicates good film coverage, minimizing shunting paths between TiO_2 and the spiro-OMeTAD that would otherwise be present. The EQE shown in Figure 3b is not indicative of the high J_{SC} reported as it was measured at lower illumination intensity. The purpose of the EQE spectrum was to discuss the exciton absorption peak at the band edge as above. Therefore, only the standard spectral response measurement set up for larger area crystalline silicon photovoltaic device with lower than 1 sun monochromatic light was used without light bias.

To summarize, we report a vapor-assisted method for fabricating $CH_3NH_3PbBr_3$ perovskite film for solar devices. The films exhibit long carrier diffusion length exceeding 1 μm. A solar device employing this film has been demonstrated achieving averaged (from forward and reverse scans) conversion efficiency of 8.7%, V_{oc} of 1.45 V, J_{sc} of 9.75 mA/cm^2, and fill factor of 61.5%. Compared to one-step solution process, the vapor-assisted process results in better film quality in terms of crystallinity, uniformity, coverage, and light absorption, hence resulting in better photovoltaic performance in the associated devices. The high voltage output of this device makes it a good candidate for tandem solar cell application.

EXPERIMENTAL METHODS

CH_3NH_3Br was synthesized following a previously reported method[19] by mixing methylamine (33% in methanol, Sigma-Aldrich) with hydrobromic acid (48% in water, Sigma-Aldrich) in a 1:1 molar ratio in a 250 mL round-bottom flask under continuous stirring at 0 °C for 2 h. The precipitate was recovered by rotary evaporation at 60 °C and then washed three times with diethyl ether in an ultrasonic bath for 30 min. The final product was collected after dehydration at 60 °C and placed in a vacuum chamber for overnight.

Solar cell devices were fabricated on fluorine-doped tin oxide (FTO)-coated glass (Pilkington, 8 Ω/sq). FTO was patterned with 2 M HCl and zinc powder. Substrates were then cleaned in 2% Hallmanex detergent, acetone, and isopropanol in an ultrasonic bath for 10 min in each cleaning agent followed by UVO treatment for 10 min. The compact TiO_2 layer was deposited by spin-coating a mildly acidic solution of titanium isopropoxide in ethanol at 2500 rpm for 60 s followed by annealing at 500 °C for 30 min. The mp-TiO_2 layer composed of 20 nm sized particles was deposited by spin-coating at 2000 rpm for 60 s using a commercial TiO_2 paste (Dyesol 18NRT, Dyesol) diluted in ethanol (2:7, weight ratio). After being dried at 125 °C, the TiO_2 film was heated to 500 °C, annealed at this temperature for 30 min, and gradually cooled to room temperature.

$CH_3NH_3PbBr_3$ films were deposited using the vapor-assisted method. First, $PbBr_2$ solution in DMF with a concentration of 1 M was spin-coated on the mp-TiO_2 at 2500 rpm for 60 s. After annealing at 70 °C for 30 min, the film was treated by CH_3NH_3Br vapor at 150 °C for 10 min in a closed glass Petri dish with CH_3NH_3Br powder surrounded on a hot plate in glovebox and then rinsed in isopropanol at room temperature.

To complete the solar devices, HTM was then deposited by spin-coating at 2000 rpm for 60 s. The solution was prepared by dissolving 72.3 mg of 2,2′,7,7′-tetrakis(*N*,*N*-di-*p*-methoxyphenylamine)-9,9′-spirobifluorene (spiro-MeOTAD), 28.8 mL of 4-*tert*-butylpyridine (4-TBP), and 17.5 mL of a stock solution of 520 mg/mL lithium bis(trifluoromethane)-sulfonimide (LiTFSI) in acetonitrile in 1 mL of chlorobenzene. The samples were left overnight in dry air before 100 nm gold contacts were thermally evaporated on the back through a shadow mask. The device fabrications were carried out under controlled atmospheric condition and a humidity of 1 ppm.

X-ray diffraction (XRD) patterns were measured using a PANalytical Xpert Materials Research diffractometer system with a Cu Kα radiation source (λ = 0.1541 nm) at 45 kV and 40 mA.

The current density−voltage (J−V) measurements were performed using an IV5 solar cell I−V testing system from PV measurements, Inc. (using a Keithley 2400 source meter), under illumination power of 100 mW/cm^2 by an AM1.5G solar simulator (Oriel model 94023A).

Reflectance (R) and transmittance (T) of this $CH_3NH_3PbBr_3$ film were measured using a Varian Cary UV−vis−NIR spectrophotometer at close to normal incidence. The optical properties, in particular the imaginary part of the dielectric constant (ε_2), was determined by modeling with the computer software WVASE. The real part of the dielectric constant (ε_1) was extracted from ε_2 using the Kramers−Kronig (KK) method. The real and imaginary parts of the refractive index (n and k, respectively) were determined from the relationships

$$\varepsilon_1 = n^2 - k^2; \quad \varepsilon_2 = 2nk \tag{1}$$

The absorption coefficient α of the film was then calculated:

$$\alpha = \frac{4\pi k}{\lambda} \tag{2}$$

The tr-PL were measured by a microtime200 microscope (Picoquant) using the TCSPC technique with an excitation of 470 nm laser at 4 MHz repetition rate and a detection at 536 nm.[26]

The charge carrier diffusion length (L_D) in the perovskite layer is calculated from eq 3

$$L_D = \sqrt{D\tau_e} \tag{3}$$

where τ_e is the recombination lifetime of charge carriers in the nonquench perovskite film and D is the diffusion coefficient. τ_e is determined by fitting tr-PL of the nonquenched perovskite film with a stretched exponential decay function as shown in the following:

$$I(t) = I_0 \exp\left(-\frac{t}{\tau_e}\right)^{\beta} \tag{4}$$

In order to determine the diffusion coefficient, one-dimensional diffusion equation is used to calculate the number and distribution of the charge carrier density which is generated by the laser pulse[18−20]

$$\frac{\partial n(x,t)}{\partial t} = D\frac{\partial^2 n(x,t)}{\partial x^2} - kn(x,t) \tag{5}$$

DOI: 10.1021/jp512936z
J. Phys. Chem. C XXXX, XXX, XXX−XXX

where k is the PL decay rate of the perovskite film without any quenching layer and $k = \beta\tau_e^{-\beta}t^{\beta-1}$ and $n(x,t)$ is the charge carrier density. The notation "x" represents the distance from the perovskite surface to a point inside the perovskite layer and $x = 0$ at the perovskite surface. The notation "t" is a time coordinate.

The 1-D diffusion coefficient has two boundary conditions. The first boundary condition assumes the photoexcited charge carriers are generated on the perovskite surface; the initial distribution of the charge carriers is expressed by the equation

$$n(x, 0) = n_0 e^{-\alpha x} \quad (6)$$

where α is the absorption coefficient of the perovskite film at 470 nm. The second boundary condition assumes the quench process appears only at the TiO_2/perovskite or spiro-OMeTAD/perovskite interface, and all the charge carriers are quenched in this interface. The boundary condition can be expressed as

$$n(L, t) = 0 \quad (7)$$

where L is the thickness of perovskite.

The carrier density $n(x,t)$ and the total charge density $N(t)$ (see eqs S1 and S2 in the Supporting Information) can be solved by using 1-D diffusion equation and the boundary conditions.

Finally, the diffusion coefficient is obtained by fitting the $N(t)$ and the tr-PL measured from the quench interface.

■ ASSOCIATED CONTENT

Supporting Information

Comparison of $CH_3NH_3PbBr_3$ films and associated solar devices prepared by one-step solution-based method and vapor-assisted method; tr-PL fitting equations. This material is available free of charge via the Internet at http://pubs.acs.org.

■ AUTHOR INFORMATION

Corresponding Author

*E-mail: a.ho-baillie@unsw.edu.au (A.H.-B.).

Notes

The authors declare no competing financial interest.

■ ACKNOWLEDGMENTS

The Australian Centre for Advanced Photovoltaics (ACAP) encompasses the Australian-based activities of the Australia-US Institute for Advanced Photovoltaics (AUSIAPV) and is supported by the Australian Government through the Australian Renewable Energy Agency (ARENA). Responsibility for the views, information, or advice expressed herein is not accepted by the Australian Government.

■ REFERENCES

(1) Green, M. A.; Ho-Baillie, A.; Snaith, H. J. The emergence of perovskite solar cells. *Nat. Photonics* **2014**, *8* (7), 506−514.

(2) Singh, S. P.; Nagarjuna, P. Organometal halide perovskites as useful materials in sensitized solar cells. *Dalton Trans.* **2014**, *43* (14), 5247−5251.

(3) Kojima, A.; et al. Organometal halide perovskites as visible-light sensitizers for photovoltaic cells. *J. Am. Chem. Soc.* **2009**, *131* (17), 6050−6051.

(4) Green, M. A. Perovskite Single-Junction and Silicon- or CIGS-Based Tandem Solar Cells: Hype or Hope?. In *Proc. of 29th EU PVSEC 2014*, Amsterdam, The Netherlands, 22−26 Sept 2014.

(5) Heo, J. H.; Song, D. H.; Im, S. H. Planar $CH_3NH_3PbBr_3$ hybrid solar cells with 10.4% power conversion efficiency, fabricated by controlled crystallization in the spin-coating process. *Adv. Mater.* **2014**, *26*, 8179−8183.

(6) Noh, J. H.; et al. Chemical management for colorful, efficient, and stable inorganic−organic hybrid nanostructured solar cells. *Nano Lett.* **2013**, *13* (4), 1764−1769.

(7) Edri, E.; et al. High open-circuit voltage solar cells based on organic−inorganic lead bromide perovskite. *J. Phys. Chem. Lett.* **2013**, *4* (6), 897−902.

(8) Ryu, S.; et al. Voltage output of efficient perovskite solar cells with high open-circuit voltage and fill factor. *Energy Environ. Sci.* **2014**, *7* (8), 2614−2618.

(9) Chen, Q.; et al. Planar heterojunction perovskite solar cells via vapor-assisted solution process. *J. Am. Chem. Soc.* **2013**, *136* (2), 622−625.

(10) Eperon, G. E.; et al. Morphological control for high performance, solution-processed planar heterojunction perovskite solar cells. *Adv. Funct. Mater.* **2014**, *24* (1), 151−157.

(11) Xiao, M.; et al. A fast deposition-crystallization procedure for highly efficient lead iodide perovskite thin-film solar cells. *Angew. Chem.* **2014**, *126* (37), 10056−10061.

(12) Huang, F.; et al. Gas-assisted preparation of lead iodide perovskite films consisting of a monolayer of single crystalline grains for high efficiency planar solar cells. *Nano Energy* **2014**, *10* (0), 10−18.

(13) Dualeh, A.; et al. Effect of annealing temperature on film morphology of organic−inorganic hybrid pervoskite solid-state solar cells. *Adv. Funct. Mater.* **2014**, *24* (21), 3250−3258.

(14) Burschka, J.; et al. Sequential deposition as a route to high-performance perovskite-sensitized solar cells. *Nature* **2013**, *499* (7458), 316−319.

(15) Liu, M.; Johnston, M. B.; Snaith, H. J. Efficient planar heterojunction perovskite solar cells by vapour deposition. *Nature* **2013**, *501* (7467), 395−398.

(16) Jeon, N. J.; et al. Solvent engineering for high-performance inorganic−organic hybrid perovskite solar cells. *Nat. Mater.* **2014**, *13* (9), 897−903.

(17) Snaith, H. J.; et al. Anomalous hysteresis in perovskite solar cells. *J. Phys. Chem. Lett.* **2014**, *5* (9), 1511−1515.

(18) Edri, E.; et al. Chloride inclusion and hole transport material doping to improve methyl ammonium lead bromide perovskite-based high open-circuit voltage solar cells. *J. Phys. Chem. Lett.* **2014**, *5* (3), 429−433.

(19) Aharon, S.; Cohen, B. E.; Etgar, L. Hybrid lead halide iodide and lead halide bromide in efficient hole conductor free perovskite solar cell. *J. Phys. Chem. C* **2014**, *118* (30), 17160−17165.

(20) Tanaka, K.; et al. Comparative study on the excitons in lead-halide-based perovskite-type crystals $CH_3NH_3PbBr_3$ $CH_3NH_3PbI_3$. *Solid State Commun.* **2003**, *127* (9−10), 619−623.

(21) Bai, S.; et al. High-performance planar heterojunction perovskite solar cells: Preserving long charge carrier diffusion lengths and interfacial engineering. *Nano Res.* **2014**, 1−10.

(22) Stranks, S. D.; et al. Electron-hole diffusion lengths exceeding 1 micrometer in an organometal trihalide perovskite absorber. *Science* **2013**, *342* (6156), 341−344.

(23) Xing, G.; et al. Long-range balanced electron- and hole-transport lengths in organic-inorganic $CH_3NH_3PbI_3$. *Science* **2013**, *342* (6156), 344−347.

(24) Hanusch, F. C.; et al. Efficient planar heterojunction perovskite solar cells based on formamidinium lead bromide. *J. Phys. Chem. Lett.* **2014**, *5* (16), 2791−2795.

(25) Heo, J. H.; et al. Efficient inorganic−organic hybrid heterojunction solar cells containing perovskite compound and polymeric hole conductors. *Nat. Photonics* **2013**, *7*, 486−491.

(26) Wen, X.; et al. Morphology and carrier extraction study of organic−inorganic metal halide perovskite by one- and two-photon fluorescence microscopy. *J. Phys. Chem. Lett.* **2014**, *5* (21), 3849−3853.

DOI: 10.1021/jp512936z
J. Phys. Chem. C XXXX, XXX, XXX−XXX